ChemSusChem

Research Article
doi.org/10.1002/cssc.202102180

Chemistry Europe
European Chemical Societies Publishing

www.chemsuschem.org

Electrified Conversion of Contaminated Water to Value: Selective Conversion of Aqueous Nitrate to Ammonia in a Polymer Electrolyte Membrane Cell

Sorin Bunea,[a] Kevin Clemens,[a] and Atsushi Urakawa*[a]

The application of a polymer electrolyte membrane (PEM) electrolytic cell for continuous conversion of nitrate, one of the contaminants in water, to ammonia at the cathode was explored in the present work. Among carbon-supported metal (Cu, Ru, Rh and Pd) electrocatalysts, the Ru-based catalyst showed the best performance. By suppressing the competing hydrogen evolution reaction at the cathode, it was possible to reach 94% faradaic efficiency for nitrate reduction towards ammonium. It was important to match the rate of the anodic reaction with the cathodic reaction to achieve high faradaic efficiency. By recirculating the effluent stream, 93% nitrate conversion was achieved in 8 h of constant current electrolysis at 10 mA cm^{-2} current density. The presented approach offers a promising path towards precious NH_3 production from nitrate-containing water that needs purification or can be obtained after capture of gaseous NO_x pollutants into water, leading to waste-to-value conversion.

Introduction

NH_3 production by the Haber-Bosch process is the main pillar of the fertilizer manufacturing industry. About 170 million tonnes of ammonia are produced yearly, and in 2008 nitrogen-containing fertilizers derived from NH_3 were responsible for feeding 48% of the world's population.[1] It is predicted that crop production needs to be increased by 100% by 2050 to meet the global food demand, and so does the ammonia production capacity.[2] However, the widely practiced Haber-Bosch process is unsustainable due to the use of hydrogen originating from fossil fuel and the energy-intensive steam reforming process to produce hydrogen.[3] As a consequence, CO_2 emissions associated with the Haber-Bosch process account for 1% of the global annual CO_2 emissions.[4] The process can be made greener when the hydrogen is produced using renewable energies. Still, there is a relatively large intrinsic energy requirement of the process due to the high-temperature and high-pressure conditions of the Haber-Bosch process.

With increasing availability of renewable and natural energy sources, which are accessible as electric power in most processes, the electrochemical synthesis of ammonia from nitrogen [Eq. (1)] has attracted significant attention in the last decade.[1a,5] Nevertheless, the reported product yields are still far from industrial relevance, due to challenges related to nitrogen activation.

$$N_2(g) + 8\,H^+ + 6\,e^- \rightleftharpoons 2\,NH_4^+(aq)\ (pH < 9.25);\quad E^\circ = 0.27\,V\ (vs.\ RHE) \tag{1}$$

Besides, there is another issue associated with increasing ammonia production. The use of nitrogen-containing fertilizers has led to an increase of nitrate ion (simply called nitrate or NO_3^-) concentration in the soil and groundwater. It has to be removed to prevent environmental (eutrophication) and human health (e.g., methemoglobinemia) consequences. Furthermore, highly polluting nitrate-containing waste streams are generated from various industrial processes such as uranium purification, saltpeter mining and metal finishing, where the abatement of the contaminants is crucial to minimize the environmental impacts.[6]

In this regard, electrochemical conversion of nitrate to ammonia, which can be present as ammonium ion (simply called ammonium or NH_4^+) in water [Eq. (2)], offers a unique solution to this problem, by the possibility to convert the undesired chemical waste to a valuable product. This approach allows closing the agricultural nitrogen cycle and contributing towards a circular economy when the process is sourced by renewable energies. In a more ambitious approach, the large amounts of NO_x gases generated by fossil fuel power plants, which can be absorbed in liquid solutions as nitrate and nitrite, could be reduced electrochemically to ammonia.[7]

$$NO_3^- + 10H^+ + 8\,e^- \rightarrow NH_4^+ + 3\,H_2O;\quad E^\circ = 0.88\,V\ (vs.\ NHE) \tag{2}$$

[a] S. Bunea, K. Clemens, Prof. Dr. A. Urakawa
Catalysis Engineering, Department of Chemical Engineering
Delft University of Technology
Van der Maasweg 9, Delft, 2629 HZ (The Netherlands)
E-mail: A.Urakawa@tudelft.nl

Supporting information for this article is available on the WWW under https://doi.org/10.1002/cssc.202102180

This publication is part of a Special Collection highlighting "The Latest Research from our Board Members". Please visit the Special Collection.

The electrochemical nitrate reduction has been extensively investigated for potential water treatment applications, where nitrogen is the main targeted reaction product [Eq. (3)].[8]

$$2\,NO_3^- + 12\,H^+ + 10\,e^- \rightarrow N_2 + 6\,H_2O;\quad E^\circ = 1.25\,V\ (\text{vs. NHE}) \tag{3}$$

Fundamental studies on the electrochemical nitrate reduction towards nitrogen at various noble and non-noble metal electrodes have been reported in literature.[9] The electrochemical conversion of nitrate to ammonia has gained interest only recently as a potential solution for nitrate valorization, and faradaic efficiencies (FEs) of up to 100% were achieved.[10] Still, for the commercialization and large-scale operation of the process, it is important to be able to perform the reaction in flow electrolysis cells at high FE and high selectivity towards ammonia/ammonium, at the same time reaching high single-pass conversion.

The nitrate reduction reaction to nitrogen has been implemented in a polymer electrolyte membrane (PEM) flow cell, with high nitrate conversion and selectivity towards nitrogen reported using Cu, Ni, Pt, and Pd electrodes.[11] This represents an important step towards the large-scale application of an electrochemical denitrification process. However, in the PEM cell the reaction is suggested to proceed via an electrolysis-assisted process in which nitrate ions are not electrochemically reduced at the cathode surface, but rather hydrogenated by the hydrogen evolved at the cathode in the hydrogen evolution reaction (HER) [Eq. (4)].[12]

$$2\,H^+ + 2\,e^- \rightarrow H_2;\quad E^\circ = 0\,V\ (\text{vs. NHE}) \tag{4}$$

High product yields can be obtained by operating the PEM cell in a high-current regime, thus promoting heterogeneous nitrate hydrogenation. Still, the FE of such an approach is low due to high HER activity. On the other hand, it is well known that ammonia/ammonium formation from nitrate is favored at low electrolyte pH, which is the case for membranes typically used in PEM electrolysis cells.[13] Therefore, with an appropriate choice of the cathode catalyst and by suppressing the competing HER, high FEs of nitrate reduction to ammonia in PEM cells should be achievable. A schematic representation of a PEM cell applied to electrochemical nitrate reduction is presented in Figure 1.

Recently, the electrochemical nitrate reduction to ammonia in an alkaline flow cell has been reported.[10b] The main motivation for the choice of an alkaline cell is the disfavored hydrogen evolution in alkaline media compared to acidic media, which should lead to higher FE of nitrate reduction products.[14] Although 100% FE for ammonia was obtained, the use of a liquid alkaline, often corrosive, electrolyte represents a significant environmental issue and possibly hinders a large-scale application of alkaline cells. Furthermore, considering the preferable acidic environment for ammonia formation from nitrate, the use of alkaline cells is counterintuitive. In a batch cell, the positive influence of low electrolyte pH and high nitrate concentration on ammonia formation was shown, reaching 82% FE.[6]

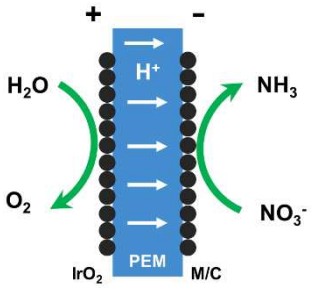

Figure 1. Schematic representation of the electrochemical nitrate reduction in a PEM electrolysis cell.

Therefore, for an electrochemical nitrate-to-ammonia process, enabling the reaction at high efficiency in a flow-through PEM electrolysis cell would be an important step towards the large-scale application. In this study, after identifying an active and selective catalyst, we show how the FE can be improved by controlling the amount of protons travelling through the PEM and thus matching the rate of nitrate reduction with that of HER.

Results and Discussion

Metal effects on nitrate reduction towards ammonia

Most studies on electrochemical nitrate reduction to ammonia available in literature focus on the investigation of metallic electrodes in three-electrode cell assemblies.[9d,15] On the other hand, PEM cells typically require the use of powdered electrocatalysts attached to PEM like Nafion. We synthesized and compared four different carbon-supported metal catalysts, namely Cu/C, Pd/C, Rh/C, and Ru/C. The characterization of the catalysts by X-ray diffraction (XRD), transmission electron microscopy (TEM), and N_2 physisorption are summarized in the Supporting Information. These active metals were chosen based on the reported activity towards nitrate reduction to ammonia and conversion of nitrates to nitrogen in PEM cells. The catalytic performance of metal-free carbon support confirms very small ammonium formation (Figures S1 and S2 in the Supporting Information). Pd is known to be active towards nitrate reduction to nitrogen, and in this context ammonia formation was viewed as the undesired reaction.[11b] Rh and Ru were reported to yield ammonia as the major reaction product, with Rh reported to be the most active in three-electrode cells using metallic electrodes.[9d] Recently, 100% FE towards ammonia was reported over strained ruthenium nanoclusters.[16] A copper nanowire array electrode yielded 95.8% FE.[10a] Nevertheless, the performance of these materials was only tested in conventional H-cells, difficult to be translated to industrial applications.

At the anode, iridium oxide was coated over the Nafion membrane at the loading of 2 mg cm^{-2}, which is typical for PEM electrolysis cells targeting water splitting for hydrogen produc-

tion. XRD study confirmed that the catalyst consists solely of IrO_2 (Figure S3). The anode reaction follows Equation (5).

$$2\,H_2O \rightarrow O_2 + 4\,H^+ + 4\,e^-; \quad E^\circ = 1.23\,V\ (\text{vs. NHE}) \tag{5}$$

Considering the half reaction of the nitrate reduction to ammonium at the cathode and the water oxidation half reaction at the anode, a theoretical cell potential of −0.36 V is expected [Eqs. (2) and (5)]. However, experimentally an overpotential is required to drive the reaction, mainly due to the sluggish kinetics of the anode reaction. Electrocatalytic performance of the four catalysts was compared in a wide cell potential range from 1.6 to 2.8 V.

Figure 2 presents nitrate conversion, product selectivity, and FE towards ammonium formation using the four carbon-supported metal catalysts. The selectivity values shown here reflect the reaction selectivity towards nitrogen-containing species. Nitrogen was the only gaseous product that contained nitrogen and could be detected by online mass spectrometry (MS). Thus, the product analysis was based mainly on the liquid-phase analysis by ion chromatography. On the other hand, the FE reflects electron selectivity, which also includes the formation of hydrogen.

The nitrate conversion increased in the order: Rh/C < Pd/C < Cu/C < Ru/C (Figure 2a). Nitrate conversion increased at higher cell potential for all catalysts except Rh/C, for which we recorded a roughly constant conversion (20%) independent of cell potential. Considering that the nitrate conversion of the carbon support ranged between 10–20% (Figure S2), the added value of Rh seems marginal. This was unexpected, as Rh is reported as the most active noble metals for nitrate reduction in acidic electrolyte.[9d]

All catalysts exhibited an increase in ammonium selectivity at higher cell potential, reaching approximately 90% for Ru/C (Figure 2b, c, e, f). However, the ammonium selectivity increase was accompanied by a decrease in FE at higher cell potential and higher current density (Figure 2b–f, Figure S4). At 2.4–2.8 V the FE was decreased to < 1% for all catalysts, accompanying vigorous bubble formation at the cathode. Online MS of the outlet gas feed indicated H_2 as the only detectable product. This suggests that ammonium is produced via an electrolysis-assisted hydrogenation pathway (i.e., nitrate reacting with produced H_2) at the high cell potential, while at 1.6–2.0 V cell potential the reaction likely follows an electrochemical pathway. The electrolysis-assisted route has been reported for nitrogen formation.[11c] In principle, heterogeneous hydrogenation of nitrate to ammonia is also feasible in a PEM cell.[12b,17]

At 1.6 V, Cu/C exhibited the highest FE of 42%, but this value dropped to around 11% at 2.0 V. Cu/C exhibited lower selectivity to side-products than Pd/C and Rh/C, but higher than Ru/C (Figure 2b, c, e, f). The general good performance of the Cu/C catalyst for ammonium formation implies that Cu is a promising non-noble metal catalyst for the reaction, and further research, for example using Cu alloys, would be of interest.

Interestingly, Pd/C showed very low FE for ammonia production over the entire range of the cell potentials (Figure 2d). Nevertheless, ammonium selectivity reached approximately 65% at 2.8 V cell potential, which indicates that ammonium can be produced over Pd via an electrolysis-assisted hydrogenation pathway (Figure 2c).

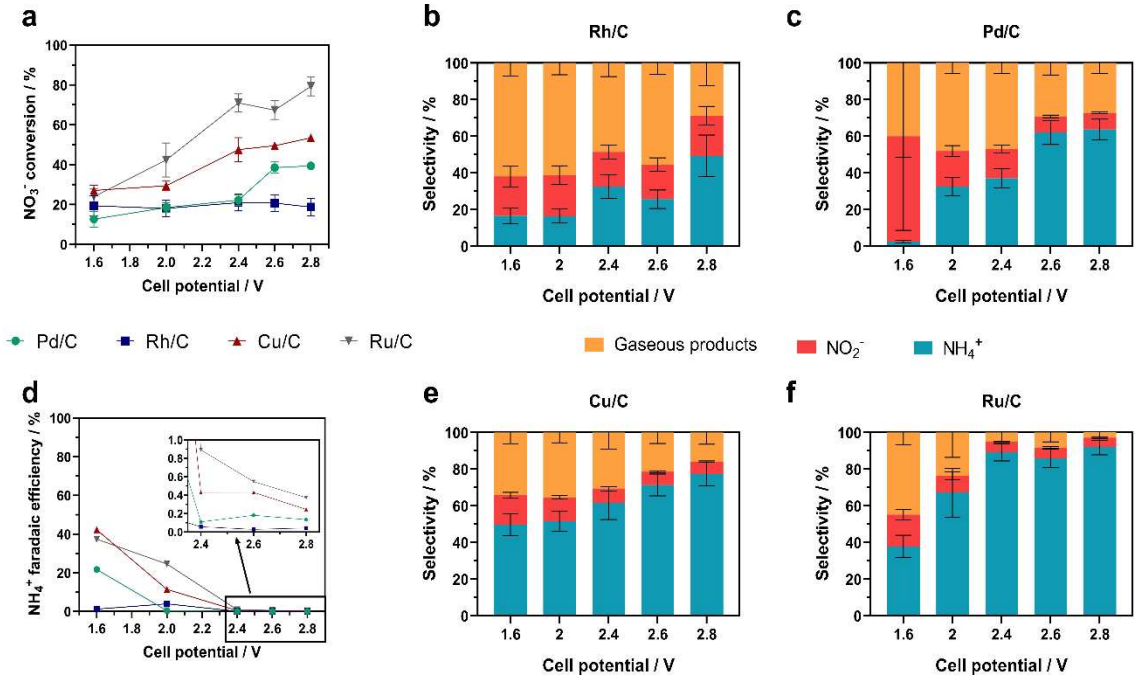

Figure 2. (a) Nitrate conversion, (d) ammonium FE, and (b, c, e, f) selectivity towards nitrogen-containing species as a function of cell potential for four different carbon-supported metal catalysts.

Among the four catalysts, Ru/C showed the best FE towards ammonium over the wide range of the cell potential. This, in addition to the highest nitrate conversion and ammonium selectivity, motivated us to investigate the possibility of improving the FE of Ru/C by controlling the amount of protons recombining to hydrogen at the cathode.

Furthermore, overpotential analysis of the polarization curves was carried out to determine the kinetic overpotentials of the four metals (Figure S5, Table S2). Due to challenges in implementing a reference electrode in the PEM electrolysis cells, it is difficult to disentangle the corresponding contributions from the reactions taking place at the cathode and anode. Hence, the apparent Tafel slopes reflect the reactions taking place at both electrodes. Nevertheless, considering that all the parameters except the cathode catalyst metal were identical, the plots in Figure S5 are useful for comparison purposes of the membrane electrode assemblies used. The metal that exhibited the highest kinetic overpotential, Ru, shows the highest activity in nitrate reduction. At the same time, Rh shows the lowest kinetic overpotential for HER, making it a poor catalyst for nitrate reduction. This is in good agreement with literature, which shows that Rh is one of the most active metals to catalyze the HER.[18] Based on the kinetic overpotential analysis, lower overpotential values are linked to higher HER rate in comparison to the nitrate reduction. The latter is more kinetically hindered unless HER is disfavored over the surface. Ru seems to achieve this condition by increasing the kinetic overpotential for HER.

Improving FE and single-pass nitrate conversion to ammonia with Ru/C

When PEM electrolysis cells are used for water splitting, an increase in iridium oxide loading typically leads to higher current densities and higher HER rates in the cell. Increasing the amount of catalyst at the anode leads to a higher surface area available for water molecules to adsorb and undergo oxidation, hence a higher recorded current at the same applied cell voltage. In other words, a lower iridium oxide loading should yield lower current densities by limiting the oxidation reaction and thus restricting the amount of protons generated at the anode and transported to the cathode. Previous experiments indicated hydrogen evolution as the main cause for low FE towards nitrate reduction products, and we decided to investigate whether this approach would be able to improve the FE. We therefore decreased the iridium oxide loading from 2 to 0.3 mg cm^{-2} and shifted the applied cell potentials towards a lower range, from 1.2 to 2.1 V. To increase the nitrate single-pass conversion and to increase the effective reaction time in the cell, the nitrate solution flow was decreased from 1 to 0.5 mL min^{-1}.

To investigate the influence of nitrate concentration on the cell performance, we tested three different initial nitrate solution concentrations: 200, 500, and 1000 ppm (Figure 3). Interestingly, regardless of nitrate concentration, there is a maximum in the FE around 1.8 V. Increasing the cell potential further drastically decreased the efficiency. Higher FE was

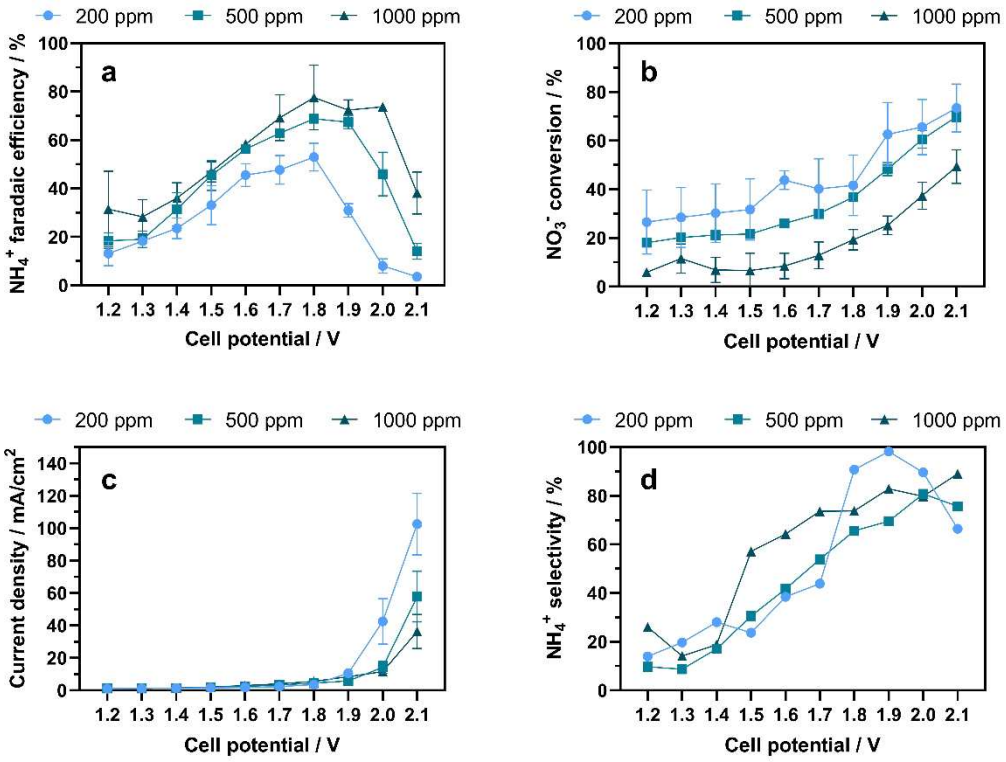

Figure 3. (a) FE towards ammonium, (b) single pass nitrate conversion, (c) current density, and (d) ammonium selectivity for solutions of different initial nitrate concentration as a function of cell potential, Ru/C cathode catalyst, 0.3 mg cm^{-2} iridium oxide anode loading.

observed for more concentrated nitrate solutions (53, 69, and 78% for 200, 500, and 1000 ppm solutions, respectively), indicating that high nitrate concentration at the catalyst surface is important to achieve efficient utilization of electrons towards ammonia/ammonium formation. A similar relation between solution concentration and faradaic efficiency was also reported by McEnaney et al.[6]

In terms of the current density, in the 1.2–1.8 V range, the measured values were comparable (<10 mA cm^{-2}) for the three cases. On the other hand, in the 1.9–2.1 V range, the current density increased for all cases, with the steepest change for the 200 ppm solution, followed by the 500 and 1000 ppm solutions (Figure 3b). This tendency is consistent with the concentration effects on the maximum FE at 1.8 V (see above), indicating that a higher HER rate is observed when the surface nitrate concentration is lower. In other words, by increasing the surface nitrate concentration, the reaction selectivity can be tuned towards ammonium even at high cell potentials.

The single-pass conversion in the PEM cell was also affected by the variation of reactant concentration. The highest conversion was observed in the experiments with 200 ppm initial nitrate solution concentration, reaching 74% at 2.1 V (Figure 3c). For the 1000 ppm nitrate solution, the conversion was the lowest, not exceeding 50% at 2.1 V. The amount of converted nitrate increased with concentration from 200 to 500 ppm. Changing the concentration to 1000 ppm did not result in a further increase in the amount of converted nitrate compared to the 500 ppm case in the 1.2–1.8 V range. At higher cell potentials, differences between the converted nitrate amount became more noticeable between the 500 and 1000 ppm solutions, with more nitrate transformed at higher concentration. This may suggest that at high cell potentials nitrate conversion proceeds via a different or an additional mechanism, as a slight decrease in ammonia selectivity was also observed in this potential range (Figure S6). For example, the reaction rate might be enhanced by the activated electrolysis-assisted path.

Mass transport overpotential as function of concentration was determined from overpotential analysis (Figure S7). In general, higher mass transport overpotential was observed at higher nitrate concentrations. At cell potentials of >1.9 V, HER becomes dominant over nitrate reduction according to the FE, and the concentration dependency implies that higher nitrate concentration hinders the HER. This is explained by the higher surface nitrate concentration and consequent kinetic hindrance of HER at the electrode surface.

Overall, our approach of decreasing the anode catalyst loading is effective, drastically improving the ammonium FE of Ru/C by approximately 38% (Figure 2d vs. Figure 3a) to 69% at 1.8 V for the 500 ppm nitrate solution. Importantly, the current density during the experiments with 0.3 mg cm^{-2} IrO_2 loading was one order of magnitude lower than that recorded for the membrane electrode assembly (MEA) with 2 mg cm^{-2} IrO_2 loading at the anode. At cell potentials higher than 2.0 V, a sharp drop in the FE was observed, accompanied by an increase in the current density for the undesired use of the electrons for HER. We have shown the possibility to reach high single-pass nitrate conversions and ammonium FEs at the low current densities and demonstrated the facile electrochemical activation of nitrate and the favorable reaction kinetics with the Ru catalyst despite the involvement of 8 electrons for the conversion. Such "mild" electrochemical conditions with the high reaction performance suggest promising prospects for the industrial implementation of an electrochemical nitrate to ammonium/ammonia process.

The highest recorded energy efficiency of nitrate reduction to ammonia was 15% for the 1000 ppm solution at 1.8 V (Figure S8).

Maximizing ammonium FE by changing the anode reaction from water oxidation to hydrogen oxidation

So far, we demonstrated to tune the current density and proton transport through the membrane electrolyte by decreasing the catalyst loading, and hence the number of active sites for water dissociation and oxidation. From a different point of view, it should be possible to control the proton transport by limiting the amount of water at the anode. For this aim, we conducted electrolysis experiments using water vapor as anode feed. Unfortunately, we were not successful in obtaining reproducible, reliable results. An underlying reason could be the uncontrolled water condensation inside our PEM cell. As an alternative approach, we replaced water oxidation taking place at the anode by hydrogen oxidation for generating protons at the anode. This has a great advantage since the hydrogen concentration in the gas flow can be more precisely controlled. Furthermore, by using a Pt-based catalyst and at low current densities, the anode can be considered a pseudo-reference reversible hydrogen electrode (RHE), which allows for a better understanding of how the working electrode (cathode) potential influences the nitrate reduction reaction.

As expected, the potentials at which comparable current densities were achieved were considerably lower, as the hydrogen oxidation reaction overpotential is considerably lower than the overpotential of the water oxidation reaction. In principle, coupling nitrate reduction to ammonia at the cathode and hydrogen oxidation at the anode yields a theoretical cell potential of 0.88 V. Experimentally, an open circuit potential (OCP) of approximately 0.6 V was observed, but we were not able to identify ammonium formation under OCP conditions. Application of cathodic potentials was required to drive ammonia formation, likely due to the existence of overpotential in the cell.

We investigated the reaction performance for the three different concentrations of nitrate solution (Figure 4), similar to the previous experiments (Figure 3). We passed a humidified 4% hydrogen feed to the anode compartment at 5 mL min^{-1}. Under these conditions, the amount of hydrogen undergoing dissociation, and the amount of protons available and traveling through the membrane towards the cathode compartment is strongly limited. This was reflected by the low current densities recorded during the experiments, which did not exceed approximately 7 mA cm^{-2}. They did not increase with applied

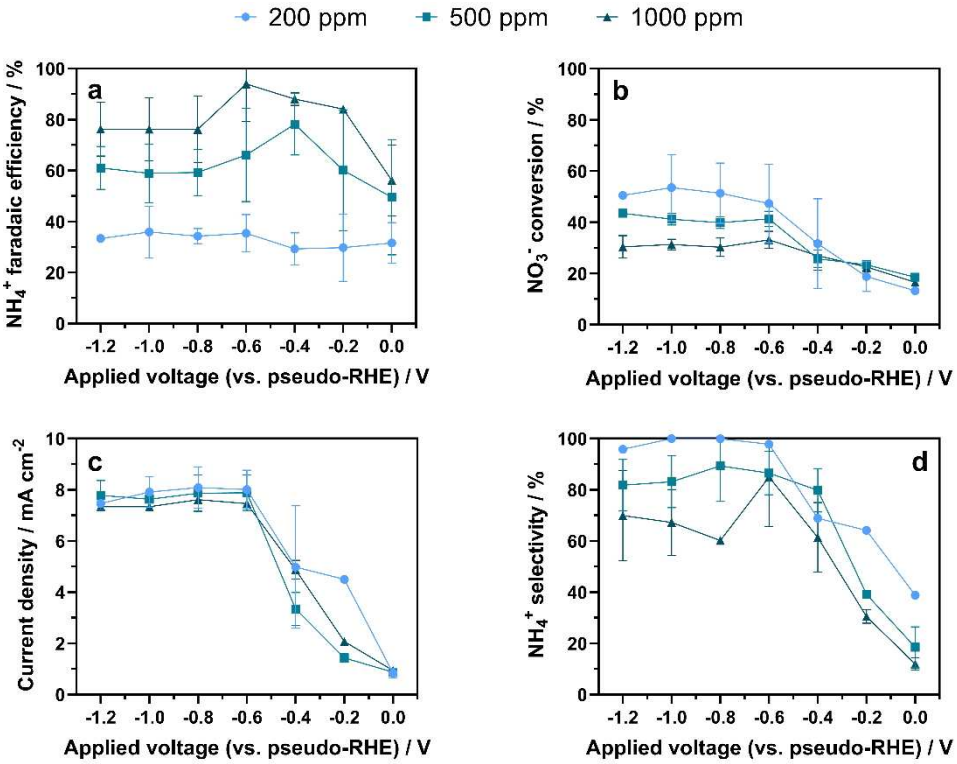

Figure 4. (a) FE towards ammonium, (b) nitrate conversion, (c) current density, and (d) ammonium selectivity for Ru/C cathode catalyst, Pt/C anode catalyst, and 5 mL min^{-1} humidified 4% H_2/He flow.

potential between −0.6 and −1.2 V vs. pseudo-RHE (Figure 4a). The trend observed earlier regarding the FE was found for solutions of different nitrate concentrations, decreasing in the order: 1000 > 500 > 200 ppm. For the 1000 ppm nitrate solution, a remarkably high FE of 94% for ammonium was observed. This confirms the positive effects of higher nitrate concentration at the catalyst surface on the ammonium FE.

Generally, the observed FE values were higher than when water oxidation took place at the anode. Conversely, the current densities at which maximum FE was observed were lower in experiments with hydrogen oxidation: 7.5 mA cm^{-2} at −0.6 V vs. pseudo-RHE (94% FE) compared to 8.4 mA cm^{-2} at 1.9 V cell potential (78% FE) for the 1000 ppm nitrate solution, and 3.34 mA cm^{-2} at −0.4 V vs. pseudo-RHE (78% FE) compared to 4.49 mA cm^{-2} at 1.9 V (69% FE) for the 500 ppm nitrate solution. The increase in the FE with decreasing current densities suggests a lower HER rate in the experiments with hydrogen oxidation at the anode and even more efficient use of electrons towards ammonium formation.

For the 200 ppm nitrate solution, the observed maximum FE was lower than in the case of water oxidation at the anode. On the other hand, the current density in the experiments with water oxidation was lower for the 200 ppm nitrate solution, 2–3 mA cm^{-2} at maximum FE (48%). When hydrogen oxidation was used as the anode reaction, the current density was approximately 7 mA cm^{-2} at maximum FE (35%) at −0.6 V vs. pseudo-RHE. The lower FE could be due to a higher extent of HER, induced by the poorer availability of nitrate at the catalyst surface.

Notably, the difference in the cell potential values at which the maximum FE was obtained for the two cases (water oxidation vs. hydrogen oxidation) was around 1.3 V. This is close to the theoretical potential of 1.23 V required for water oxidation at the anode. This is an indirect proof that the reaction is electrochemically driven by the cathodic potential when the FE is high. Furthermore, the electrochemical nitrate reduction to ammonia can be operated at a considerably lower cell potential when external hydrogen supply is used. This mode of operation allows avoiding the use of the expensive iridium oxide as water oxidation catalyst.

Interestingly, the FE towards ammonium decreased in the potential range of −0.8 to −1.2 V vs. pseudo-RHE for the 500 ppm and 1000 ppm nitrate solution (Figure 4a). This decrease in FE was not accompanied by a substantial change in current density, which was limited by the low hydrogen flow at the anode. This may be due to a change in selectivity of nitrate reduction as a function of applied potential. No nitrite formation was observed during the experiments with hydrogen oxidation at the anode as well (Figure S9), and thus this decrease in FE can be attributed to formation of gaseous nitrate reduction products, although they could not be detected in this work.

The nitrate conversion showed an increase down to −0.6 V vs. pseudo-RHE and did not increase further at more negative potentials (Figure 4b). Considering the rather constant current

densities observed in the potential range of −0.6 to −1.2 V due to limited availability of protons, this observation supports the hypothesis of a hydrogenation pathway for ammonia formation in this potential range. The highest conversion was observed for the 200 ppm nitrate solution (≈50%). The conversion showed a decrease with increasing solution concentration, reaching approximately 30% for the 1000 ppm nitrate solution, consistent with previous experiments with water oxidation at the anode, and indicating the impact of nitrate concentrations on its availability on the catalyst surface.

In the experiments with hydrogen oxidation at the anode, we were able to reach almost 100% FE for the 1000 ppm nitrate solution, proving that high FEs for electrochemical transformations in a PEM cell are possible. The highest energy efficiency of 70% was reached at −0.2 V vs pseudo-RHE (Figure S10). Solutions of higher nitrate concentration are expected to yield higher FE towards ammonium. The most critical element to reach high FEs was proved to be precise control of the current density, and hence, the proton transport through the membrane. This is necessary to suppress HER by limiting the hydrogen availability at the anode.

Maximizing nitrate conversion by cathode solution recirculation

Depending on the source of nitrate streams, nitrate concentrations vary, and flexible strategies are required to achieve desired nitrate conversions, ideally to ammonium in our case. A practical solution to influence the reaction time is to recirculate the solution through the cell. To test whether achieving full nitrate conversion by this approach is feasible, we conducted an 8 h, 10 mA cm^{-2} constant-current electrolysis experiment, during which 30 mL of a 1000 ppm nitrate solution was recirculated at a flow rate of 0.5 mL min^{-1} through the cathode compartment of the cell. In this experiment, water oxidation was the anode reaction. The nitrate conversion showed a steady increase over the reaction duration and reached 93% after 8 h (Figure 5). The selectivity towards ammonium increased from 61% after the first hour of reaction to 75% after 8 h. The recorded FE towards ammonium was 46% after 1 h of reaction and decreased to 26% after 8 h. The decrease in the FE can be attributed to a lower nitrate concentration in the recirculated solution as the reaction proceeded and more severe competition with HER.

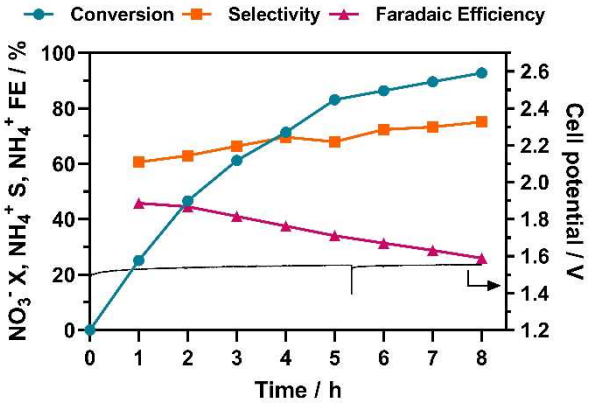

Figure 5. Nitrate conversion (X), ammonium faradaic efficiency (FE), selectivity (S), and the recorded cell potential for an 8 h recirculation experiment with 1000 ppm nitrate solution, 10 mA cm^{-2} constant-current electrolysis.

A notable detail of this experiment was that HCl was added to the nitrate solution recirculated at the cathode, for an efficient trapping of ammonia in form of ammonium ion in the liquid phase. The amount of added HCl was 2.4 mmol, to account for an 80 mM acid concentration in the reaction flask. The addition of the acid led to a decrease in cell potential from 1.90 to 1.5 V. It is well established that the nitrate reduction reaction is more favorable in acidic environment, which is the case for the Nafion membrane that we used in our cell. Nevertheless, a pH gradient between the nitrate solution flowing into the cell and the membrane exists. The nitrate solution that we typically used showed pH values between 6 and 7. With the acid addition, the pH of the solution decreased to around 1.1. The observation of the lower cell potential of this experiment hints at the importance of the nitrate solution pH passed into the electrolyzer, besides the membrane pH.

Furthermore, the cell potential increased by 4.25 mV h^{-1}, which suggests a promising long-term stability of the cell. The performance degradation in PEM cells depends on many factors, including the stability of current collector material, iridium oxide anode catalysts, and Nafion membrane besides water impurities. The optimization of long-term stability of PEM cells is therefore part of a broader field, out of the scope of the current study.

The recirculation operation mode was proved efficient in reaching >90% nitrate conversion in the PEM cell. Due to the addition of HCl, ammonia is present in form of ammonium chloride after the 8 h experiment. The recovery of ammonia gas from ammonium chloride can be achieved by stripping at alkaline pH values.

Conclusion

Continuous electrochemical nitrate reduction to ammonia in a polymer electrolyte membrane (PEM) electrolyzer was investigated. Ru was found as an active and selective cathode metal catalyst for the reaction. We were able to suppress the hydrogen evolution reaction (HER) by regulating the amount of protons transporting through the PEM and could reach almost full faradaic efficiency (FE) as high as 94% towards ammonium. Proton transport was controlled by tuning the amount and thus activity of the anode catalyst for water oxidation, or by passing controlled amount of H_2 at the anode. The results indicate the importance of optimizing the counter-electrode reaction to reach high efficiency in electrocatalytic transformations using PEM cells, an aspect that is often overlooked in literature on scaling up of electrochemical reactions. Although further investigation is necessary, direct electrocatalytic transformation of nitrate to ammonium was hinted at lower cell potential up to the point where the FE towards ammonium formation reaches

maximum. Above the cell potential reaching the maximum, the reaction is apparently dominated by the electrolysis-assisted hydrogenation, namely nitrate hydrogenation by H_2 produced in the PEM cell. Furthermore, the availability of the nitrate ions near the catalyst surface plays a vital role in defining the FE: the higher the concentration, the higher the efficiency. This poses a practical challenge to convert low concentration nitrate solution or reaching full nitrate conversion where HER is difficult to be suppressed. In such a case, by precisely regulating proton transport and using hydrogen at the anode, one can still achieve good and selective conversion of nitrate to ammonia/ammonium.

Experimental Section

Catalyst synthesis

Pd/C, Cu/C, Rh/C, and Ru/C catalyst powders were synthesized by the sodium borohydride reduction method, as described for Cu/C and Pd/C elsewhere.[19] Vulcan XC-72 carbon black from Cabot Corporation was used as catalyst support. The metal precursor, $PdCl_2$ (Alfa Aesar, 99.9%), $Cu(NO_3)_2$ (Sigma-Aldrich, 99.5%), $RhCl_3$ hydrate (Sigma-Aldrich, 99.98%), or $RuCl_3$ hydrate (Precious Metals Online, 99%), was added to a suspension of 100 mg Vulcan XC-72 in 100 mL water. The amount of precursor was calculated so that the final catalyst loading would be 40 wt%. The mixture was stirred for 1 h at room temperature. Subsequently, the reaction flask was transferred to an ultrasonic bath and a 6-fold molar excess of $NaBH_4$ powder was added. When bubble evolution stopped, the catalysts were washed by filtration, and dried at 90 °C overnight. The iridium oxide powder was synthesized following a modified Adams fusion method described elsewhere.[20]

Catalyst characterization

Conductive Vulcan XC-72 carbon black, typically used as a catalyst support both in PEM fuel cells and electrolyzers, was chosen as the support of the active metals due to its excellent electrical conductivity, high surface area, inertness, and facile dispersibility of the resulting catalyst in the inks to be deposited over the Nafion membrane. Powder XRD was used to identify the crystalline phase of the metals in the catalysts (Figure S11). The Vulcan XC-72 support, due to its amorphous structure, exhibits only a broad peak in the XRD pattern around $2\theta = 28°$. Based on XRD, Pd, Rh, and Ru are present in the metallic form. Reflections characteristic to CuO were identified in the Cu-based catalyst. Nevertheless, for the sake of brevity, the catalyst was denoted as Cu/C. Particle size and distribution of the active metals vary for each catalyst as indicated by TEM micrographs (Figure S12). Rh formed agglomerated clusters of nanoparticles (8–40 nm) over the support. More uniform distribution of Pd in Pd/C was observed, with Pd particle size between 5 and 30 nm. CuO forms platelets which form agglomerates as large as 100 nm, with a poorer dispersion. Ru/C forms spherical nanoparticles ranging from 2 to 6 nm, exhibiting the most uniform distribution among all catalysts, although some agglomerates as large as 20 nm were observed. The Brunauer–Emmett–Teller (BET) surface area of the catalyst powders (122–168 $m^2 g^{-1}$) measured by nitrogen physisorption is smaller than the surface area of the carbon support (238 $m^2 g^{-1}$). This indicates the deposition of metal nanoparticles over the carbon support, as the nanopores in the carbon support are partially blocked by the nanoparticles, leading to a decrease in surface area (Table S1).

MEA preparation

Nafion 115 (simply called Nafion hereafter) membranes (Ion Power) were activated by a three-step procedure: 1 h treatment in 3 wt% H_2O_2 solution at 80 °C, 1 h treatment in 1 M H_2SO_4 solution at 80 °C and 1 h treatment in boiling type I ultrapure water. The synthesized catalyst powders were suspended in inks containing 2 mL of isopropanol and Nafion ionomer. The amount of ionomer in the ink was 30 wt% of the catalyst loading. The inks were sonicated for 10 min in an ultrasonic bath and were deposited onto Nafion 115 membranes by spray coating. A loading of 2.5 mg cm^{-2} was used for cathode catalyst powders. The anode catalyst inks were prepared in a similar fashion. For the anode, iridium oxide powder was used. The amount of ionomer in the ink was 20 wt% of the catalyst loading. For experiments with hydrogen oxidation at the anode, a commercial 40 wt% Pt/C powder (Sigma-Aldrich) was used to prepare the ink. The loading of the Pt/C catalyst was 0.75 mg cm^{-2}. The ionomer loading in the ink was the same as for the carbon-supported catalyst powders (30 wt%). After spraying, the membranes were hot pressed at 120 °C, at a pressure of 1 MPa, for 3 min. The prepared catalyst coated membranes were sandwiched between two 2×2 cm^2 Pt-coated 0.45 mm thick Ti felt gas diffusion layers (GDLs) (68% porosity, Bekaert) and assembled in an in-house designed PEM cell with titanium current collectors and machined serpentine flow channels.

Electrochemical nitrate reduction experiments and product analysis

A peristaltic pump was used to pump KNO_3 solution of different concentrations to the cathode compartment of the PEM cell. Type I ultrapure water was passed to the anode compartment. For experiments with hydrogen oxidation at the anode, a humidified 4 vol% H_2/He mixture was passed through the anode compartment at a flow rate of 5 mL min^{-1}. The cell temperature was kept at 80 °C during experiments. The electrochemical experiments were performed using an AUTOLAB PGSTAT302N potentiostat/galvanostat. Potentiostatic and galvanostatic experiments were performed for a duration of 30 min, over which the current and the potential were recorded, respectively.

Electrochemical impedance spectroscopy experiments were conducted using a FRA32 impedance module equipped to the potentiostat/galvanostat. Spectra were recorded at 1.5 V cell voltage, with a 10 mV sinusoidal signal perturbation in the 100 kHz–100 mHz frequency range.

The reactor outlet tube was immersed in 20 mL of 20 mM HCl solution, in order to trap gas phase ammonia in form of ammonium ion and ensure a reliable quantification of reaction products. The quantification of liquid species was performed using a Metrohm 883 Basic ion chromatograph. A Metrosep C6 column was used for the quantification of ammonium, and a Metrosep A Supp 4 column was used for the quantification of nitrate and nitrite anions. The formed gas-phase products were not quantified; online MS studies did not indicate the formation of nitrogen oxides. Thus, we assumed dinitrogen to be the majority gas phase product of electrochemical nitrate reduction.

A flow of 1 mL min^{-1} and a 500 ppm nitrate (KNO_3) solution were used during the screening experiments. In experiments with decreased IrO_2 loading, the flow was set at 0.5 mL min^{-1}. Three different nitrate concentration solutions (200, 500, and 1000 ppm), were used to study concentration effects. For the recirculation experiment, 30 mL of KNO_3 solution containing 1000 ppm NO_3^- in 80 mM HCl was used. 1 mL liquid samples were collected hourly over the duration of the experiment. The higher concentration of

HCl solution used is motivated by the higher amount of ammonia produced over the 8 h experiment as the 20 mM HCl solution was inefficient to trap the produced ammonia in the liquid phase for reliable quantitative analysis.

Nitrate conversion and ammonium selectivity were calculated based on the nitrogen balance. The FE towards ammonium was calculated using Equation (S1). The energy efficiency was calculated using Equation (S2).

Overpotential analysis

The overpotential analysis was conducted according to the procedure reported for PEM electrolysis cells described elsewhere.[21] Figure S13 provides an example of how the kinetic, ohmic, and mass transport overpotentials were determined. Tafel slopes and ohmic resistance values determined from impedance spectroscopy are presented in Table S2. Recorded impedance spectra are presented in Figure S14.

Catalyst characterization

The synthesized catalyst powders were characterized by N_2 physisorption using a Micromeritics Tristar 3020, after an overnight degassing procedure at 150 °C. Powder XRD patterns were recorded using a Bruker D8 ADVANCE X-ray diffractometer with a CoK_α radiation source. TEM micrographs were recorded using a Jeol JEM-1400 plus TEM.

Conflict of Interest

The authors declare no conflict of interest.

Keywords: ammonia synthesis · catalysis · electrochemistry · nitrate reduction · PEM electrolysis

[1] a) G. Soloveichik, *Nat. Catal.* **2019**, *2*, 377–380; b) J. W. Erisman, M. A. Sutton, J. Galloway, Z. Klimont, W. Winiwarter, *Nat. Geosci.* **2008**, *1*, 636–639.
[2] X. Zhang, E. A. Davidson, D. L. Mauzerall, T. D. Searchinger, P. Dumas, Y. Shen, *Nature* **2015**, *528*, 51–59.
[3] "Ammonia, 2. Production Processes": M. Appl, in *Ullmann's Encyclopedia of Industrial Chemistry*, Wiley, Hoboken, **2011**.
[4] L. K. Boerner, in *Chemical & Engineering News, Vol. 97*, American Chemical Society, **2019**.
[5] a) A. R. Singh, B. A. Rohr, J. A. Schwalbe, M. Cargnello, K. Chan, T. F. Jaramillo, I. Chorkendorff, J. K. Nørskov, *ACS Catal.* **2017**, *7*, 706–709; b) J. G. Chen, R. M. Crooks, L. C. Seefeldt, K. L. Bren, R. M. Bullock, M. Y. Darensbourg, P. L. Holland, B. Hoffman, M. J. Janik, A. K. Jones, M. G. Kanatzidis, P. King, K. M. Lancaster, S. V. Lymar, P. Pfromm, W. F. Schneider, R. R. Schrock, *Science* **2018**, *360*, eaar6611; c) J. Deng, J. A. Iñiguez, C. Liu, *Joule* **2018**, *2*, 846–856; d) V. Kyriakou, I. Garagounis, A. Vourros, E. Vasileiou, M. Stoukides, *Joule* **2020**, *4*, 142–158; e) S. Z. Andersen, V. Čolić, S. Yang, J. A. Schwalbe, A. C. Nielander, J. M. McEnaney, K. Enemark-Rasmussen, J. G. Baker, A. R. Singh, B. A. Rohr, M. J. Statt, S. J. Blair, S. Mezzavilla, J. Kibsgaard, P. C. K. Vesborg, M. Cargnello, S. F. Bent, T. F. Jaramillo, I. E. L. Stephens, J. K. Nørskov, I. Chorkendorff, *Nature* **2019**, *570*, 504–508; f) Y.-C. Hao, Y. Guo, L.-W. Chen, M. Shu, X.-Y. Wang, T.-A. Bu, W.-Y. Gao, N. Zhang, X. Su, X. Feng, J.-W. Zhou, B. Wang, C.-W. Hu, A.-X. Yin, R. Si, Y.-W. Zhang, C.-H. Yan, *Nat. Catal.* **2019**, *2*, 448–456; g) X. Guo, H. Du, F. Qu, J. Li, *J. Mater. Chem. A* **2019**, *7*, 3531–3543; h) C. Tang, S.-Z. Qiao, *Chem. Soc. Rev.* **2019**, *48*, 3166–3180.
[6] J. M. McEnaney, S. J. Blair, A. C. Nielander, J. A. Schwalbe, D. M. Koshy, M. Cargnello, T. F. Jaramillo, *ACS Sustainable Chem. Eng.* **2020**, *8*, 2672–2681.
[7] Y. Sun, X. Hong, T. Zhu, X. Guo, D. Xie, *Appl. Sci.* **2017**, *7*, 377.
[8] M. Duca, M. T. M. Koper, *Energy Environ. Sci.* **2012**, *5*, 9726–9742.
[9] a) V. Rosca, M. Duca, M. T. de Groot, M. T. M. Koper, *Chem. Rev.* **2009**, *109*, 2209–2244; b) M. Dortsiou, G. Kyriacou, *J. Electroanal. Chem.* **2009**, *630*, 69–74; c) I. Katsounaros, M. Dortsiou, C. Polatides, S. Preston, T. Kypraios, G. Kyriacou, *Electrochim. Acta* **2012**, *71*, 270–276; d) G. E. Dima, A. C. A. de Vooys, M. T. M. Koper, *J. Electroanal. Chem.* **2003**, *554–555*, 15–23.
[10] a) Y. Wang, W. Zhou, R. Jia, Y. Yu, B. Zhang, *Angew. Chem. Int. Ed.* **2020**, *59*, 5350–5354; *Angew. Chem.* **2020**, *132*, 5388–5392; b) Y. Wang, A. Xu, Z. Wang, L. Huang, J. Li, F. Li, J. Wicks, M. Luo, D.-H. Nam, C.-S. Tan, Y. Ding, J. Wu, Y. Lum, C.-T. Dinh, D. Sinton, G. Zheng, E. H. Sargent, *J. Am. Chem. Soc.* **2020**, *142*, 5702–5708; c) P. H. van Langevelde, I. Katsounaros, M. T. M. Koper, *Joule* **2021**, *5*, 290–294.
[11] a) M. Machida, K. Sato, I. Ishibashi, M. A. Hasnat, K. Ikeue, *Chem. Commun.* **2006**, *7*, 732–734; b) M. A. Hasnat, I. Ishibashi, K. Sato, R. Agui, T. Yamaguchi, K. Ikeue, M. Machida, *Bull. Chem. Soc. Jpn.* **2008**, *81*, 1675–1680; c) J. Ampurdanés, S. Bunea, A. Urakawa, *ChemSusChem* **2021**, *14*, 1534–1544.
[12] a) M. A. Hasnat, R. Agui, S. Hinokuma, T. Yamaguchi, M. Machida, *Catal. Commun.* **2009**, *10*, 1132–1135; b) I. Katsounaros, G. Kyriacou, *Electrochim. Acta* **2008**, *53*, 5477–5484.
[13] J. Yang, P. Sebastian, M. Duca, T. Hoogenboom, M. T. M. Koper, *Chem. Commun.* **2014**, *50*, 2148–2151.
[14] T. Cheng, L. Wang, B. V. Merinov, W. A. Goddard, *J. Am. Chem. Soc.* **2018**, *140*, 7787–7790.
[15] a) K. Bouzek, M. Paidar, A. Sadílková, H. Bergmann, *J. Appl. Electrochem.* **2001**, *31*, 1185–1193; b) G. E. Dima, G. L. Beltramo, M. T. M. Koper, *Electrochim. Acta* **2005**, *50*, 4318–4326; c) S. Taguchi, J. M. Feliu, *Electrochim. Acta* **2007**, *52*, 6023–6033; d) M. Li, C. Feng, Z. Zhang, N. Sugiura, *Electrochim. Acta* **2009**, *54*, 4600–4606; e) M. Li, C. Feng, Z. Zhang, Z. Shen, N. Sugiura, *Electrochem. Commun.* **2009**, *11*, 1853–1856; f) E. Pérez-Gallent, M. C. Figueiredo, I. Katsounaros, M. T. M. Koper, *Electrochim. Acta* **2017**, *227*, 77–84.
[16] J. Li, G. Zhan, J. Yang, F. Quan, C. Mao, Y. Liu, B. Wang, F. Lei, L. Li, A. W. M. Chan, L. Xu, Y. Shi, Y. Du, W. Hao, P. K. Wong, J. Wang, S.-X. Dou, L. Zhang, J. C. Yu, *J. Am. Chem. Soc.* **2020**, *142*, 7036–7046.
[17] a) X. Huo, D. J. Van Hoomissen, J. Liu, S. Vyas, T. J. Strathmann, *Appl. Catal. B* **2017**, *211*, 188–198; b) L. Wei, D.-J. Liu, B. A. Rosales, J. W. Evans, J. Vela, *ACS Catal.* **2020**, *10*, 3618–3628.
[18] S. Trasatti, *J. Electroanal. Chem. Interfacial Electrochem.* **1972**, *39*, 163–184.
[19] O. M. Ilinitch, F. P. Cuperus, L. V. Nosova, E. N. Gribov, *Catal. Today* **2000**, *56*, 137–145.
[20] S. Siracusano, V. Baglio, S. A. Grigoriev, L. Merlo, V. N. Fateev, A. S. Aricò, *J. Power Sources* **2017**, *366*, 105–114.
[21] T. Schuler, T. J. Schmidt, F. N. Büchi, *J. Electrochem. Soc.* **2019**, *166*, F555–F565.

Manuscript received: October 11, 2021
Revised manuscript received: November 15, 2021
Accepted manuscript online: November 22, 2021
Version of record online: December 9, 2021